Biochimica et Biophysica Acta 1858 (2016) 1926–1934

Contents lists available at ScienceDirect

Biochimica et Biophysica Acta

journal homepage: www.elsevier.com/locate/bbamem

Stratum corneum lipid matrix: Location of acyl ceramide and cholesterol in the unit cell of the long periodicity phase

E.H. Mojumdar [a], G.S. Gooris [a], D. Groen [a], D.J. Barlow [b], M.J. Lawrence [b], B. Demé [c], J.A. Bouwstra [a,*]

[a] Leiden Academic Centre for Drug Research, Department of Drug Delivery Technology, Gorlaeus Laboratories, University of Leiden, Leiden, The Netherlands
[b] Pharmaceutical Science Division, King's College London, London, United Kingdom
[c] Institute Laue-Langevin, Grenoble, France

ARTICLE INFO

Article history:
Received 6 April 2016
Accepted 5 May 2016
Available online 8 May 2016

Keywords:
Stratum corneum
Ceramides
Lipid mixtures
Long periodicity phase
Neutron diffraction

ABSTRACT

The extracellular lipid matrix in the skin's outermost layer, the stratum corneum, is crucial for the skin barrier. The matrix is composed of ceramides (CERs), cholesterol (CHOL) and free fatty acids (FFAs) and involves two lamellar phases: the short periodicity phase (SPP) and the long periodicity phase (LPP). To understand the skin barrier thoroughly, information about the molecular arrangement in the unit cell of these lamellar phases is paramount. Previously we examined the molecular arrangement in the unit cell of the SPP. Furthermore X-ray and neutron diffraction revealed a trilayer arrangement of lipids within the unit cell of the LPP [D. Groen et al., Biophysical Journal, 97, 2242–2249, 2009]. In the present study, we used neutron diffraction to obtain more details about the location of lipid (sub)classes in the unit cell of the LPP. The diffraction pattern revealed at least 8 diffraction orders of the LPP with a repeating unit of 129.6 ± 0.5 Å. To determine the location of lipid sub(classes) in the unit cell, samples were examined with either only protiated lipids or selectively deuterated lipids. The diffraction data obtained by means of D_2O/H_2O contrast variation together with a gradual replacement of one particular CER, the acyl CER, by its partly deuterated counterpart, were used to construct the scattering length density profiles. The acyl chain of the acyl CER subclass is located at a position of ~21.4 ± 0.2 Å from the unit cell centre of the LPP. The position and orientation of CHOL in the LPP unit cell were determined using tail and head-group deuterated forms of the sterol. CHOL is located with its head-group positioned ~26 ± 0.2 Å from the unit cell centre. This allows the formation of a hydrogen bond with the ester group of the acyl CER located in close proximity. Based on the positions of the deuterated moieties of the acyl CER, CHOL and the previously determined location of two other lipid subclasses [E.H. Mojumdar et al., Biophysical Journal, 108, 2670–2679, 2015], a molecular model is proposed for the unit cell of the LPP. In this model CHOL is located in the two outer layers of the LPP, while CER EOS is linking the two outer layers with the central lipid layers. Finally the two other lipid subclasses are predominantly located in the central layer of the LPP.

1. Introduction

The skin protects us from the hazardous external environment by providing an essential barrier. In several inflammatory skin diseases, however, this barrier is impaired [1–6]. The physical barrier afforded by the skin is provided primarily by its outermost layer referred to as stratum corneum (SC) [7]. The SC consists of corneocytes (dead flattened cells filled with keratin and water) embedded in the lipid matrix. The corneocytes are surrounded by a cornified envelope which hampers the partitioning of molecules into the corneocytes. As a consequence, the intercellular lipid matrix is an important route for penetration of substances across the skin [8,9].

As the intercellular lipid domains in the SC serve as an important route for penetration of compounds, the lipid matrix plays an important role in the skin barrier function [10]. For this reason, it is essential to unravel the lipid organization. The SC lipids assemble in two co-existing crystalline lamellar phases. The aim of this study was to provide details on the lipid arrangement on a molecular level in the unit cell in one of these lamellar phases.

The main lipid classes in the SC are ceramides (CERs), cholesterol (CHOL) and free fatty acids (FFAs) in an approximately equimolar ratio [11–15]. The CERs consist of long acyl chains linked to a sphingoid base through an amide linkage. Currently 14 different CER subclasses are identified in human SC [14,16–18]. These subclasses vary in molecular architecture of both the sphingoid base and acyl chain. Four of these CER subclasses have an exceptional molecular structure with a very long

* Corresponding author at: Department of Drug Delivery Technology, Leiden Academic Centre for Drug Research, Einsteinweg 55, 2333 CC, Leiden.
E-mail address: bouwstra@chem.leidenuniv.nl (J.A. Bouwstra).

http://dx.doi.org/10.1016/j.bbamem.2016.05.006
0005-2736/

ω-hydroxy fatty acid chain ester linked to a linoleic acid, referred to as CER EO (acyl CERs). In human and pig SC, the CERs, together with CHOL and FFAs, form two co-existing crystalline lamellar phases. These two phases are referred to as the long periodicity phase (LPP) and the short periodicity phase (SPP) with a repeat distance of approximately 130 and 60 Å, respectively [19–22]. Furthermore, it has been reported that the presence of CER EO is required for the formation of the LPP [23]. As the LPP is considered to be important for the skin barrier, the presence of CER EO in the lipid composition is an important factor in maintaining the skin barrier [24]. The importance of CER EO and the LPP for the skin lipid barrier has been demonstrated by studies performed with model membranes: the absence of CER EO hampers the formation of the LPP and reduces the lipid barrier of these lipid membranes [25]. As this indicates that the LPP plays a crucial role in the skin barrier, it is thus important to unravel the molecular organization of the lipids in the unit cell of the LPP.

Studies have been reported focusing on the lipid arrangement and molecular interaction of lipids in mixtures consisting of only 3–5 lipid subclasses using neutron diffraction [26–28]. Although these studies are of great interest and provide important information on the localization of lipid subclasses in the unit cell, often the lipid phase behaviour does not mimic that in SC. In our studies we focus on more complex mixtures that form a single lamellar phase that is also present in SC. In previous studies we examined the lipid organization in the unit cell of the SPP. The location of the most abundant CER subclass, ceramide non-hydroxy sphingosine with a chain length of 24 carbon (CER NS C24, the structure is provided in Fig. S1), the FFA with a chain length of 24 carbon atoms (C24, lignoceric acid) and CHOL in the unit cell of the SPP has been determined using neutron diffraction. Based on these results a molecular model for the SPP unit cell was proposed [25,29]. As far as the LPP is concerned, a few studies are also documented in the literature regarding the arrangement of lipids in the LPP [30,31]. In one of these studies an asymmetric arrangement of the lipids in the unit cell is proposed. These studies were performed using cryo-electron microscopy combined with computer simulations. In the other study, using X-ray diffraction, a two-layer lipid arrangement is proposed in which CHOL is asymmetrically located near the outer border of each lipid bilayers in a 130 Å unit cell. In another study using X-ray diffraction, a more detailed electron density profile could be constructed showing a symmetric trilayer arrangement of lipids in the unit cell of the LPP [32].

In order to obtain the location of the lipid subclasses in the arrangement in the unit cell of the LPP, recently neutron diffraction studies were performed as well. In these studies, the water distribution in the LPP unit cell was determined. The water distribution confirmed a trilayer arrangement in the unit cell of the LPP [33]. In that study the location of two highly abundant lipids in the lipid mixtures forming only the LPP: CER NS C24 and FFA C24 are predominantly located in the central part of the unit cell.

As CER EOS (one subclass of CER EO family, see Supplemental Fig. S1 for the structure) is crucial for the formation of the LPP, it is important to locate CER EOS in the unit cell of the LPP. Therefore, in this study we focused on the location of CER EOS in the unit cell using neutron diffraction in combination with D/H contrast variation. The linoleate moiety (18 carbon atoms (C)) attached to the 30 C acyl chain of the CER EOS was perdeuterated. Furthermore, the molecular location of CHOL has also been examined. The CHOL molecules were deuterated either in the head-group region or in the tail of the molecule. First, the neutron scattering length density (SLD) profiles of the LPP were constructed using D_2O/H_2O and D/H (acyl chain CER EOS) contrast variation. Second, the location of the CER EOS linoleate moiety and the CHOL head and tail region were determined from their selectively deuterated counterparts. Finally, based on the position of these molecules together with the previously determined CER NS C24 and FFA C24 positions, a molecular model for the LPP is proposed.

2. Materials and method

2.1. Materials

In this study the following synthetic CERs were used; the ester linked omega-hydroxy acyl chain (abbreviation EO, 30 carbons in the acyl chain (C30)) with a sphingosine chain (abbreviation S, C18) referred to as CER EOS (C30), a non-hydroxy acyl chain (abbreviation N, C24) linked to a sphingosine base (C18) referred to as CER NS (C24), a non-hydroxy acyl chain (C24 or C16) linked to a phytosphingosine base (abbreviation P) referred to as CER NP (C24) and CER NP (C16) respectively, an alpha-hydroxy chain (abbreviation A) linked to a sphingosine base referred to as CER AS (C24) and an alpha-hydroxy acyl chain (C24) linked to a phytosphingosine base referred to as CER AP (C24). The number in parentheses indicates the number of carbon atoms present in the acyl chain of the CERs. All the CERs were generously provided by Evonik (Essen, Germany). Palmitic acid (C16:0), stearic acid (C18:0), arachidic acid (C20:0), behenic acid (C22:0), tricosanoic acid (C23:0), lignoceric acid (C24:0), cerotic acid (C26:0), CHOL and deuterated water were obtained from Sigma-Aldrich Chemie GmbH (Schnelldorf, Germany). The CHOL with head deuterated in the positions 2, 3, 4 and 6 (total 6 deuterium, d6-CHOL) and tail deuterated in the positions 25, 26 and 27 (total 7 deuterium, d7-CHOL) were obtained from Larodan (Malmö, Sweden). The CER EOS with its deuterated linoleate (total 31 deuterium, referred to as CER d31-EOS) was custom synthesized by Evonik (Essen, Germany) and kindly provided for this study. The molecular structure of the CER d31-EOS, d6-CHOL and d7-CHOL are presented in Fig. 1. Silicon substrates (cut from a wafer) were obtained from Okmetic (Vantaa, Finland). All solvents used were of analytical grade and supplied by Labscan (Dublin, Ireland). The water was of Millipore quality produced by Milli-Q water filtration system with a resistivity of 18 MΩ·cm at 25 °C.

2.2. Composition of the model lipid mixtures

The model lipid mixtures were prepared from synthetic CERs, CHOL and FFAs in an equimolar ratio. The CER subclasses consisted of the following CER composition; CER EOS C30, CER NS C24, CER NP C24, CER AS C24, CER NP C16 and CER AP C24 in a 13.3:12.0:3.7:1.0:2.0:1.3 molar ratio and is referred to as CERmix. This ratio resembles very closely the CER composition reported in the pig SC [34], except for CER EOS. This CER subclass is present at an increased level (4.9 molar % in case of pig SC vs 13.3 molar % in our present study). The FFA composition was prepared from seven FFA subclasses; C16:0, C18:0, C20:0, C22:0, C23:0, C24:0 and C26:0 at molar ratios of 0.6:1.3:2.6:14.2:1.7:11.5:1.4. The composition of FFA mixture is based on the FFA chain length distribution reported for SC [35]. For preparing the deuterated lipid mixtures, the protiated CER EOS and CHOL were replaced by their deuterated counterparts.

To perform contrast variation, the level of CER d31-EOS varied at the expense of CER EOS keeping the total level of CER EOS constant. Five different molar ratios of CER d31-EOS/CER EOS has been prepared which corresponds to the 0%, 25%, 50%, 75% and 100% of CER d31-EOS in the lipid mixtures. The composition of the model lipid mixtures prepared with their molar ratios and the total number of deuterated atoms per lipid molecule and the abbreviations used for these particular mixtures are provided in Table 1.

2.3. Preparation of the model lipid mixtures

The sample preparation method and the equilibration procedure for all the lipid mixtures are the same as described previously [33]. Briefly, the appropriate amount of lipids was dissolved in chloroform/methanol (2:1 v/v) solution at 10 mg/mL concentration. Subsequently the lipids were sprayed on a silicon substrate in an area of 1.2×4.0 cm^2 using a Camag Linomat IV sample applicator (Muttenz, Switzerland). After equilibrating the samples at ~70 °C, the samples were cooled and

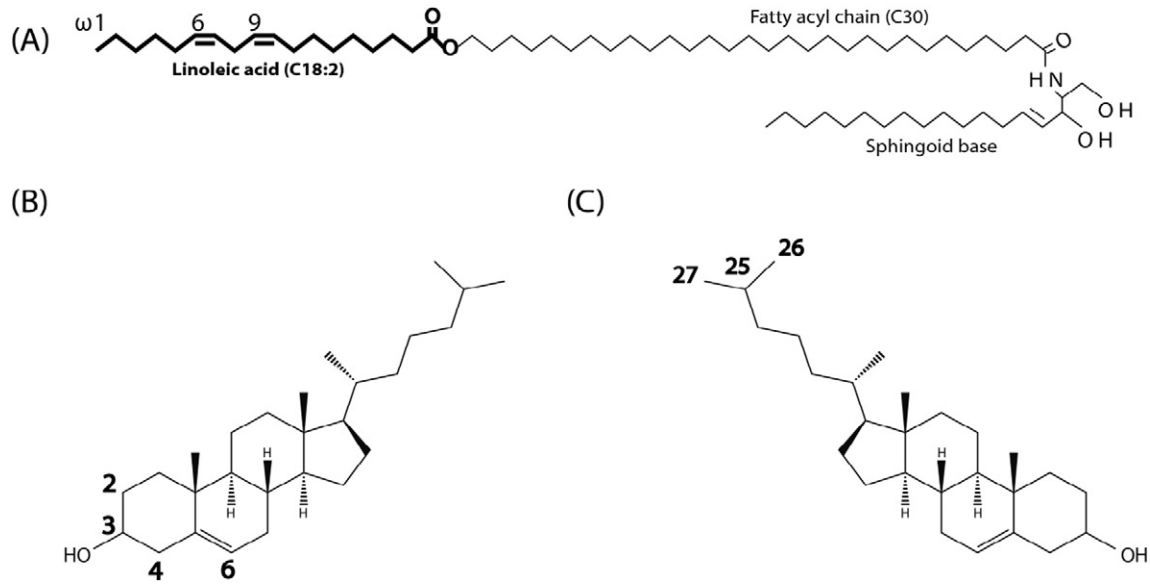

Fig. 1. The molecular structure of the deuterated lipids. A) CER EOS with its linoleate moiety deuterated (bold part, total 31 deuterium atoms, CER d31-EOS). B) CHOL with its deuterated head-group region at position 2, 3, 4 and 6 (total 6 deuterium atoms, d6-CHOL). C) CHOL deuterated in the tail of the molecule at a position of 25, 26 and 27 (total 7 deuterium atoms, d7-CHOL).

subsequently hydrated with D_2O/H_2O buffer at 100% relative humidity (RH) for about 15 h for the first time at 37 °C prior to the neutron diffraction measurement.

All the CER d31-EOS/CER EOS containing samples used for contrast variation were measured at 100% D_2O/H_2O. In addition, the LIPsc-d31-EOS sample were hydrated at additional four different D_2O/H_2O ratios; 8%, 50%, 66% and 83% D_2O/H_2O.

The samples prepared with either d6-CHOL or d7-CHOL were all measured at three different D_2O/H_2O ratios namely 8%, 66% and 100%. During the hydration steps the D_2O/H_2O ratios of the samples were randomized. The hydration period between two measurements was around 12 h.

2.4. Neutron diffraction experiment

Neutron diffraction data were collected at the D16 cold neutron diffractometer of the Institute Laue-Langevin (ILL) located in Grenoble, France. The wavelength of the neutrons 4.75 Å was achieved by the reflection of a highly ordered pyrolytic graphite (HOPG) monochromator. The sample to detector distance was 0.85 m and all the samples were measured in the reflection mode. The samples were mounted on a goniometer placed in an aluminium chamber. The temperature of the chamber was maintained at 25 °C throughout the measurements. During the sample measurements, the bottom of the chamber was filled with the same D_2O/H_2O ratio as used for hydrating the sample, to maintain a 100% RH at a constant D_2O/H_2O ratio. The measurement time per sample varied between 10 and 12 h depending on the signal/noise ratio. The neutron scattering density was recorded by a position sensitive two dimensional ^{3}He detector (320 × 320 mm area with a spatial resolution of 1 × 1 mm). The samples were measured during a series of beam line sessions. In each session a control protiated sample equilibrated at 100% D_2O/H_2O was also measured. In this way comparing the scattering length density profiles calculated for the protiated and partly deuterated samples are obtained from samples measured under the same circumstances.

2.5. Data reduction procedure

A water calibration measurement was performed to correct for the detector efficiency. An empty chamber was measured as background and subtracted from each measurement to increase the signal/noise ratio. For data analysis, the ILL in-house software LAMP was used [36]. During the measurements, the sample was rotated in steps of 0.1° from 0 to 10.5° to cover all the 8/9 diffraction orders and the detector images were taken at each step. For each diffraction order the peak intensity was integrated in a θ range of 0.4°. (−0.2 to +0.2) around θ_h the Bragg angle of the h^{th} order reflection to calculate the structure factor amplitude. For determining the repeat distances, the two dimensional detector image was vertically integrated along the detector axis (2θ) which results in one dimensional diffraction pattern of scattering intensities (I) vs scattering angle (2θ). Subsequently, the scattering angle is converted to the scattering vector (q):

$$q = \frac{4\pi \sin\theta}{\lambda}. \quad (1)$$

In this equation, θ is the Bragg angle, λ is the wavelength of the neutron beam. The repeat distance (d) was calculated from the positions of

Table 1
The lipid composition and molar ratios, the deuterated molar ratios and the total number of deuterated atoms per lipid molecule for the various lipid mixtures. The repeat distance with its standard error of all the lipid mixtures is also provided.

Abbreviation	Lipid composition and molar ratio (equimolar)	Deuterated molar ratio	No. of deuterated atoms per molecule	Repeating unit D (Å)
LIPsc*	CERmix/CHOL/FFA	0	0	129.4 ± 0.5
LIPsc-d31-EOS	CERmix (CER d31-EOS)/CHOL/FFA**	13.3	31	129.7 ± 0.3
LIPsc-d6-CHOL	CERmix/d6-CHOL/FFA	33.3	6	129.6 ± 0.3
LIPsc-d7-CHOL	CERmix/d7-CHOL/FFA	33.3	7	129.7 ± 0.4

* The neutron diffraction profile of LIPsc has also been measured and published previously [33], but is also measured in this series of studies in each session as it serves as a control.
** For contrast variation the ratio between CER d31-EOS/CER-EOS was varied.

a series of equidistant peaks attributed to the lamellar phase (q_h), in which h is the diffraction order:

$$d = \frac{2\pi h}{q_h}. \quad (2)$$

All the diffraction orders were fitted with the Gaussian function ($\phi(x)$):

$$\phi(x) = ae^{-\frac{(x-\mu)^2}{2\sigma^2}} + c. \quad (3)$$

Here, c is the offset for the baseline correction. The structure factor amplitude $|F_h|$ of each diffraction order was then calculated from the Gaussian peak height (I_h) by using the formula:

$$|F_h| = A_h\sqrt{LI_h}. \quad (4)$$

The Lorentz correction (L) values were calculated and applied to correct for the intensities. The sample absorption correction factor (A_h) was calculated using the following equation [37]:

$$A_h = \frac{1}{\sqrt{\frac{\sin\theta}{2\mu l}\left(1-e^{\frac{-2\mu l}{\sin\theta}}\right)}}. \quad (5)$$

Here μ represents the linear attenuation coefficient and l is the thickness of the lipid film. In a previous study the thickness of the lipid film was calculated to be 24 μm [29]. The attenuation coefficients were calculated using the wavelength of the neutrons in combination with the lipid density (~0.873 g/cm^3) and the chemical composition of the lipid films [38].

Previously using D_2O/H_2O contrast variation, it was reported that the LPP unit cell is centrosymmetric [33]. The water layer structure factors are defined as the structure factors at 100% D_2O/H_2O minus the structure factors at 8% D_2O/H_2O. The structure factor phase signs of the various diffraction orders of the LIPsc-d31-EOS, LIPsc-d6-CHOL and LIPsc-d7-CHOL samples were determined from the linear plot of the structure factors vs D_2O/H_2O ratios such that the difference between 100% D_2O/H_2O and 8% D_2O/H_2O corresponds to the correct phase sign for the water layer structure factor at that particular diffraction order. A more detailed description is given elsewhere [37,39,40]. In obtaining additional information on the location of CER EOS, the structure factor amplitudes were plotted as a function of CER d31-EOS/CER EOS with varying ratios between 0% and 100% for the various diffraction orders. To determine the slope of these diffraction orders, the phase signs of the structure factors derived from D_2O/H_2O contrast variation for LIPsc-d31-EOS have been used. The structure factor amplitudes for the various diffraction orders of all lipid mixtures measured at different contrast variation levels are provided in the Supplemental Table 1. The error in the structure factors is also provided. These were determined as described previously [29].

The SLD profile $\rho(x)$ across the unit cell was calculated by Fourier reconstructions:

$$\rho(x) = F_0 + 2\sum_{h=1}^{h_{max}} F_h \cos\left(\frac{2\pi hx}{d}\right). \quad (6)$$

Here, X is the direction normal to the unit cell surface and $x = 0$ is the centre of the unit cell. The scattering density per unit volume (F_0) was calculated in order to put the data on an absolute scale. Using the chemical composition of the mixture and the mass density of the sample, the F_0 was calculated for each of the lipid compositions [41,42]. The calculation of F_0 for LIPsc-d31-EOS is explained into more details in the Supplemental materials. The data were then placed on a 'relative absolute' scale [25,43–45]; the known neutron SLDs of deuterium and hydrogen were used to scale the differences in such a way so that the area differences between the SLDs is equal to the SLD of the deuterium label, for instance, 7 deuterium difference in case of CHOL deuterated tail. The difference density profiles were then constructed by subtracting the protiated profiles from the deuterated profiles. For the water profiles an absolute relative scale was not possible as in the unit cell no region is present with only water.

3. Results

The lipid mixtures measured with neutron diffraction were either protiated or contained either deuterated CER EOS (18 C linoleate moiety is deuterated) or deuterated CHOL (deuterated in the head-groups or in the tail of the molecule, see Fig. 1). The repeat distance of all the lipid mixtures measured with neutron diffraction was calculated by a least square fitting method and are provided in Table 1. The mean repeat distance of all the samples was calculated to be 129.6 ± 0.5 Å. A one dimensional intensity vs q diffraction plot for LIPsc-d31-EOS is provided in Fig. 2 showing the various diffraction orders. The pattern exhibit diffraction peaks attributed to the LPP and crystalline phase separated CHOL. No additional phases were observed. The protiated lipid mixture (LIPsc) has been reported previously [33]. In this lipid mixture, the water was not only present at the boundaries of the unit cell but also at two distinct regions inside the unit cell (~20 Å from the unit cell centre). In that publication we explained the determination of the phase signs of water in details. This is based on the contrast variation method described by Zaccai et al. 1975, Franks et al. 1979 [37,46]. Briefly, the D_2O/H_2O composition in various ratios has been used as a contrast method in order to determine the water phase signs assuming that the water molecules are located close to the hydrophilic head-group regions at the cell boundaries. This increment of D_2O/H_2O contrast in the head-group regions results in the phase signs of water − + − + − + − + − for the first 9 diffraction orders. When plotting the structure factors as a function of D_2O/H_2O for various diffraction orders, a linear fitting was observed, indicating a centrosymmetry in the structure. Besides this combination of phase signs, all other possible phase signs were also used to calculate the corresponding water distributions. Those phase sign combinations, however, resulted in an unrealistic water distribution [33].

In the present study, we performed neutron diffraction measurements of the LIPsc-d31-EOS as a function of D_2O/H_2O contrast variation. A linear relationship in the structure factor amplitudes vs D_2O/H_2O contrast variation at five different D_2O/H_2O ratios for the various diffraction orders indicate a centrosymmetric lipid arrangement in the unit cell of the LPP (Fig. 3A). In addition, we also performed contrast variation as

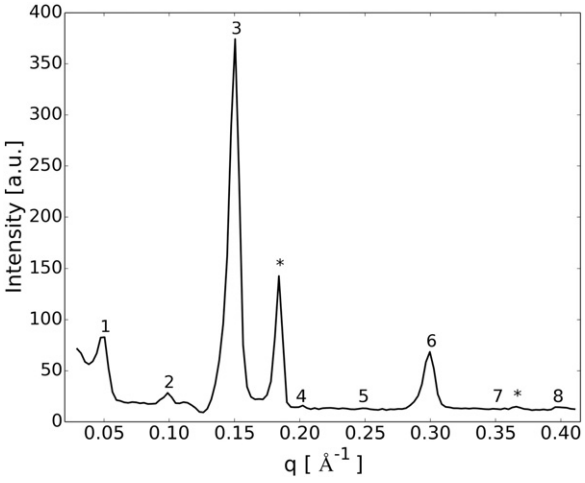

Fig. 2. Neutron diffraction one dimensional plot of intensity vs q for the LIPsc-d31-EOS hydrated and measured at 100% D_2O/H_2O. The higher diffraction orders of the LPP lamellae are indicated by the Arabic numbers and the CHOL peaks by means of an asterisk.

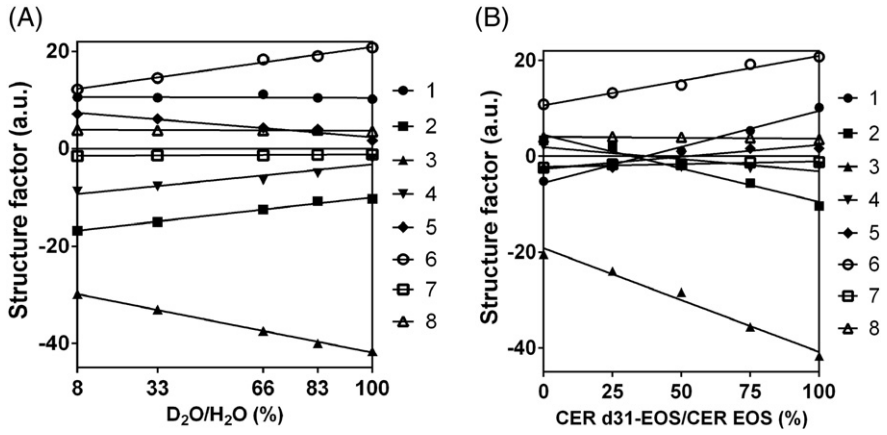

Fig. 3. Relative structure factor amplitudes of the various diffraction orders for the LIPsc-d31-EOS mixture A) as a function of D_2O/H_2O exchange ratio and B) as a function of CER d31-EOS/CER EOS contrast variation. The numbers in the plot indicate the different diffraction orders.

function of measurements for CER d31-EOS/CER EOS contrast variation. In these experiments the samples were all hydrated and measured at 100% D_2O/H_2O. A linear relation between the structure factors of these samples as a function of CER d31-EOS/CER EOS was also observed, demonstrating a centrosymmetric structure (Fig. 3B). This demonstrates that not only water, but also the linoleate moiety of CER EOS is located symmetrically in the unit cell of the LPP.

Having determined the phase signs for CER d31-EOS/CER EOS at 100%, we proceed to use them as a starting point to determine the phases of other CER d31-EOS/CER EOS containing samples as follows: First the phase signs of the LIPsc-d31-EOS were determined from the linear plot as a function of D_2O/H_2O contrast variation, using the correct water layer structure factors for the various diffraction orders. These phase signs for the first 8 orders are + − − − + + − + (Fig. 3A). Applying these phase signs to the CER d31-EOS/CER EOS contrast variation and assuming a straight line for each of the diffraction orders in the contrast variation plot in Fig. 3B results in the phase signs for the CER d31-EOS/CER EOS contrast variation samples (+ − − − + + − − for the first 8 orders). The structure factor phase signs at 0% CER d31-EOS/CER EOS measured at 100% D_2O/H_2O were also determined in our previous study [33]. When comparing these phase signs, an excellent matching is observed (− + − + − + − + for the first 8 diffraction orders), see Fig. 3B.

Based on the structure factors in combination with the phase signs and using Eq. (6), the neutron SLD profiles in the unit cell of the LPP were constructed. Fig. 4A (top) displays the SLD profiles of the LIPsc-d31-EOS constructed at 8% and 100% D_2O/H_2O. The difference between 8% and 100% D_2O/H_2O indicates the water profile (Fig. 4A, bottom plot); four elevated scattering density regions (two at the border and two inside the unit cell) are observed, indicating the positions of the hydrophilic head-groups in these regions. The position of the inside water regions in the net D_2O/H_2O profile is located at ~21 ± 0.3 Å from the unit cell centre (determined by Gaussian peak fitting procedure).

Fig. 4B depicts the SLD profiles generated for the CER d31-EOS/CER EOS mixture at 0% and 100% when hydrated and measured at 100% D_2O/H_2O. The difference profile between 0% and 100% CER d31-EOS/CER EOS shows the position of the linoleate moiety. This profile clearly indicates the maximum of the position of the linoleate in the LPP unit cell at ~21.4 ± 0.2 Å from the unit cell centre. The positions of these maxima are co-incident with those of the water maxima in the unit cell.

In order to obtain further details on the molecular arrangement in the unit cell of the LPP, the location of CHOL (deuterated head-group

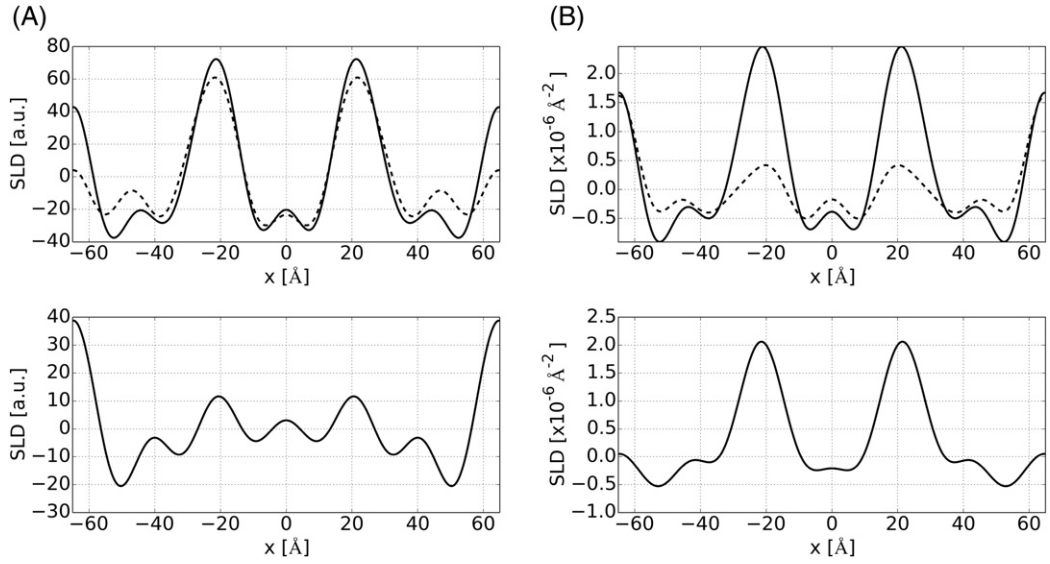

Fig. 4. A) The relative SLD profiles for the LIPsc-d31-EOS hydrated and measured at 8% (top dashed line) and 100% (top solid line) D_2O/H_2O. The difference plot between 8% and 100% D_2O/H_2O shows the water profile (bottom solid line). B) The SLD profiles constructed for 0% (top dashed line) and 100% (top solid line) CER d31-EOS/CER EOS hydrated and measured at 100% D_2O/H_2O on a relative absolute scale. The difference between the SLDs indicated by the bottom solid line shows the position of the linoleate moiety in the LPP unit cell.

and the deuterated tail region) in the LPP unit cell was also determined. Fig. 5 displays the one dimensional diffraction patterns of the scattered intensity vs q plots for LIPsc-d6-CHOL (Fig. 5A) and LIPsc-d7-CHOL (Fig. 5B) mixtures. All the diffraction peaks show a slight peak asymmetry due to the large size of the samples relative to the sample-to-detector distance, and this is most evident at the lower q values. The linear relationship between the structure factor amplitudes of various diffraction orders vs D_2O/H_2O contrast of these two lipid mixtures are shown in Supplemental Fig. S2. This linearity demonstrates that CHOL is also symmetrically located in the unit cell. Using the D_2O/H_2O contrast variation at 3 different ratios (8, 66 and 100% D_2O/H_2O), the structure factor phase signs of the various diffraction orders in the diffraction pattern of the deuterated CHOL containing lipid mixtures were determined: the difference between 100% and 8% D_2O/H_2O correspond to the correct phase signs for the water layer structure factor at that particular order. The phase signs for the first 9 diffraction orders of the deuterated CHOL containing lipid mixtures are $-+-+-+-+-$ respectively.

To locate the molecular position of the CHOL in the unit cell of the LPP, the SLD profiles of the deuterated CHOL (head group or tail) were constructed and are presented in Fig. 6 (top); LIPsc-d6-CHOL (Fig. 6A) and LIPsc-d7-CHOL (Fig. 6B) along with protiated LIPsc profiles measured previously [33] and in our current studies. The difference density profiles for the deuterated CHOL were obtained by subtracting the protiated profile either from the profile of deuterated CHOL head or from the deuterated CHOL tail profile (shown in bottom solid lines). The difference profiles show the position of the CHOL in the unit cell of the LPP; CHOL head-group resides slightly outward from the inside head-group regions at a position of ~26.0 ± 0.2 Å from the unit cell centre, with the CHOL tail ~42.0 ± 0.2 Å from the centre of the unit cell (determined after Gaussian peak fitting). Therefore, the total length over which CHOL is present in the unit cell is ~16 Å, similar to the length of CHOL.

4. Discussion

In our work, we focus on the lipid organization in the SC as the lipids play a prominent role in the skin barrier function. In previous studies, we examined the lipid organization in SC and detected two lamellar phases, the LPP and SPP [19]. In subsequent studies using lipid model systems the role the lipids play in the SC lipid organization was studied and it was observed that CERs and CHOL are crucial for the formation of the lamellar phases [47–50], while FFAs enhance the formation of an orthorhombic lateral packing [35]. Furthermore, when focusing on the CER subclasses, CER EOS is crucial for the formation of the LPP [25].

In our recent studies, our aim was to elucidate the molecular arrangement of lipids within the unit cell of the two lamellar phases. First, we examined the molecular arrangement in the unit cell of the SPP [25,29]. Using neutron diffraction in combination with contrast variation, it was possible to locate CHOL and the most abundant CER and FFA in the unit cell of the SPP. The present study is a continuation of our research focusing on the arrangement of the lipid (sub)classes in the unit cell of the LPP.

In previous studies the electron density profile of the unit cell of the LPP was determined using a sampling method based on variations in repeat distances of the LPP. This electron density profile indicates a three layer arrangement of the lipids in the unit cell [32], but the location of the lipid (sub)classes in this arrangement could not be determined. In a recent study using neutron diffraction we demonstrated a symmetric three layer arrangement very similar to that of the electron density profile obtained by X-ray diffraction [33]. In addition, the location of CER NS and FFA C24 in the unit cell of the LPP was determined. Both lipids are most abundantly present in the centre of the unit cell [33]. The aim of the present study was to determine the location of CER EOS and CHOL. These lipids are important building blocks of the LPP as it has been demonstrated that CER EOS and CHOL are both indispensable for the formation of the LPP [24,49,50]. In order to be able to form exclusively the LPP, in the present study we increased the level of CER EOS in the lipid mixtures from around 5%, the level approximately present in pig SC, to 13.3% molar fraction [51]. Indeed at this elevated CER EOS level no SPP is formed and the diffraction peaks attributed to phase separated crystalline CHOL does not interfere with the diffraction peaks assigned to the LPP. The rationale behind choosing the CER composition is explained in more details in our previous study. Furthermore, the equimolar CER:CHOL:FFA ratio is based on the composition in the SC [15]. Important to mention is the low water content in these CER mixtures [26,29,52]. In general the level of water is only 1 to 2 water molecules per lipid molecule, contrasting the situation in phospholipid bilayer systems.

4.1. Molecular model of the LPP

Based on the location of the lipids determined in our current (CER EOS and CHOL) and previous (CER NS and FFA C24) studies a molecular model for the LPP lipid lamellae is proposed (see Fig. 7) [33]. In the previous publication it was shown that CER NS and FFA C24 is predominantly present in the centre of the unit cell of the LPP with substantial interdigitation of the acyl chains [33]. In addition, there is a smaller fraction of the CER NS and FFA C24 also present starting at the unit cell border and extending into the outer cell layers. Because CER NS and FFA C24 primarily occupy space in the central lipid layer, it is expected that the CER EOS head group is located close to the unit cell border. The 30 C acyl chain of CER EOS extends from the unit cell border into the lipid layers adjacent to the cell boundary. Assuming a perpendicular orientation to the basal plane as a consequence, the ester group of CER

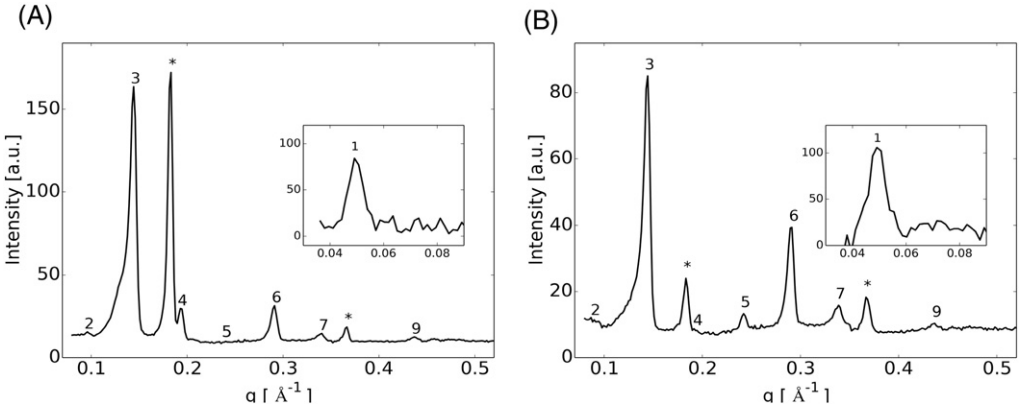

Fig. 5. One dimensional neutron diffraction plot of intensity vs q for the LIPsc-d6-CHOL (Fig. 5A) and LIPsc-d7-CHOL (Fig. 5B) hydrated and measured at 100% D_2O/H_2O. The various diffraction orders of the LPP lamellae are indicated by the Arabic numbers and the CHOL peaks by means of an asterisk. Inset; the 1st order diffraction pattern of the LIPsc-d6-CHOL and LIPsc-d7-CHOL mixtures measured at different detector position. The 8th order diffraction peak is not visible in the spectra, indicating the continuous form factor is zero at this point.

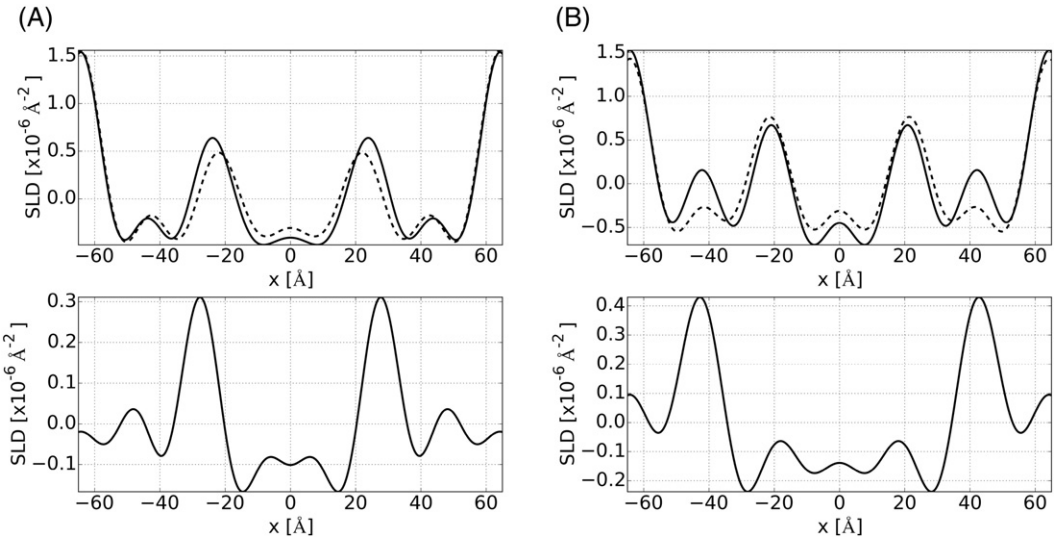

Fig. 6. The neutron SLD profiles for the A) LIPsc-d6-CHOL and B) for LIPsc-d7-CHOL mixture hydrated and measured at 100% D_2O/H_2O (top solid lines). The profiles for LIPsc mixtures at 100% D_2O/H_2O are given in dashed lines (top). The difference profiles indicating the molecular position of the CHOL head-group and tail are shown in the bottom solid lines.

EOS is located at around 37 Å from the cell boundary, very close to the position of CHOL head-group region, which is in agreement with the obtained tail and head-group position of CHOL (see next paragraph, Figs. 7 and 8). CHOL is not located in the central layer of the LPP. The location of CHOL and CER EOS is described in more details below.

4.2. Location of CHOL in the unit cell of the LPP

The head and tail positions of the sterol molecule in the SLD profiles of the LPP unit cell demonstrate that CHOL spans a distance of ~16 Å in length (evident from Gaussian peak fitting of the SLD profiles of CHOL), indicating that the molecule is oriented almost perpendicular to the basal plane (a schematic drawing of the CHOL is provided in Fig. 8). The CHOL head-group is located at a position of ~26 Å from the unit cell centre and this is around 38 Å from the unit cell boundary. Consequently the head group of CHOL is present in the same position as the ester bond of CER EOS (see next paragraph). This may allow the formation of a hydrogen bond between the –OH group of CHOL and the carbonyl group (C═O) of the CER EOS in this region. In this way the hydrophobic part of CHOL is arranged close to the saturated acyl chains of the CERs providing strong van der Waals interactions. In a previous study, an asymmetric distribution of CHOL near the outer border of the two lipid layers in the unit cell of ~130 Å was reported [31] — very close to the position of CHOL observed in the present study. However, due to the limited number of reflections used in that publication, the resolution of the electron density profile was limited which precluded observing the inner low electron density region, representing the central lipid layer in the LPP. This has been more thoroughly explained before [37]. In another work relative intensities of the diffraction peaks were calculated from an electron density stripmodel using a two bilayer arrangement. Based on the relative intensities it was shown that the electron density arrangement were expected to be symmetric, in accordance with our observations [45].

4.3. Location of CER EOS in the LPP

The maximum of the peaks attributed to LIPsc-d31-EOS in the difference profile of the SLD in the unit cell is located at ~21.4 ± 0.2 Å from the unit cell centre (evident from Gaussian peak fitting of the SLD profile as shown in Fig. 4B). This location of the SLD maximum of linoleate in the unit cell is approximately the same as the position of the inner head groups in the unit cell, which are ~20 Å from the unit cell centre [32]. The CER EOS has 30 C in its acyl chain. The ω-hydroxy moiety is ester linked to the 18 C linoleate chain, which contains two double bonds. If the head-group region of CER EOS is at the unit cell boundary, the 30 C acyl chain of CER EOS directing from the unit cell border into the direction of the centre of the unit cell extends ~37 Å (30 C × 1.25 Å) toward the unit cell centre terminating in the ester bond linking the linoleate. Based on the location of the ester bond, CER EOS linoleate extends ~7 Å (~5–6 C atoms) in the direction of the unit cell centre before it reaches the position of the highest SLD at the inner head-group region (located at 20 Å from the centre and thus 45 Å from the unit cell border). This implies a total distance between EOS ester bond and the tails of the CER NS and FFA C24 of around 17 Å. We assume that the CER EOS is located perpendicular to the basal plane, which is a realistic assumption because CHOL is located

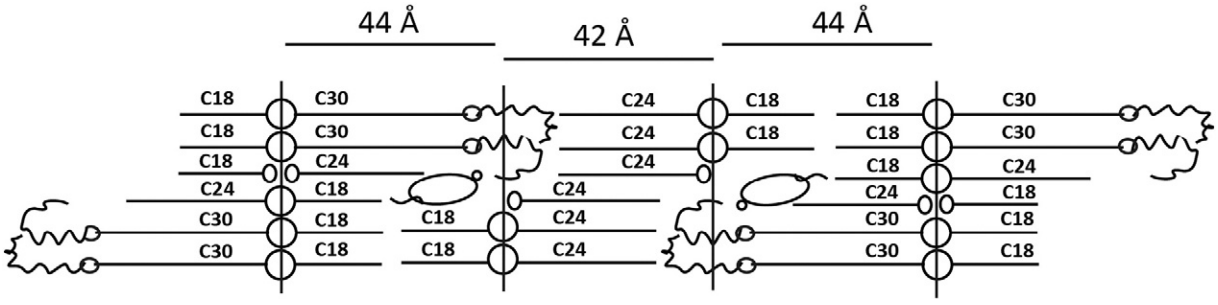

Fig. 7. The proposed molecular model of the unit cell of the LPP based on the location of lipids determined in our current and previous neutron diffraction experiments. The model is presented in fully extended conformation. However, the hairpin conformation is also possible, but then the structure is less flexible toward exchanging the position of lipids.

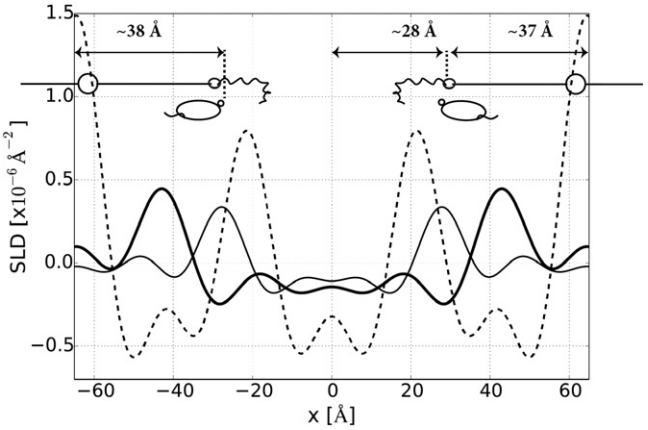

Fig. 8. A schematic drawing of the position of CER EOS and CHOL in the unit cell of the LPP. The positions are based on their difference profiles in the LPP unit cell: thin line, CHOL head deuterated and thick line, CHOL tail deuterated. The dashed line indicate LIPsc profile at 100% D_2O/H_2O. Note that, the position of the CER EOS linoleate moiety is approximately at the same position of inner head-group region of the LIPsc profile (~21 Å from the unit cell centre). This is also the location of inner water molecules within the unit cell.

perpendicular to this plane. The linoleate located in this gap exists in a highly disordered state, which is evident from the high CD_2 stretching band frequencies observed in the Fourier transform infrared spectroscopy studies with a deuterated linoleate moiety [53]. The linoleate chain, therefore, may wiggle around and also partly fold back at the position of the inner head-group regions and can compensate for two acyl chains directing from the opposite head-group regions. The location of the unsaturated linoleate moiety in the hydrophilic head-group region is unusual. However, such an arrangement may be supported by i) stabilization of CHOL that may form a hydrogen bonding with the carbonyl group, ii) due to the high conformational disordering of the linoleate, an entropic stabilization may also occur and iii) the hydrophilicity of the head-group regions is limited compared to phospholipid bilayers as the lipid matrix contain only 1–2 (bound) water molecules per lipid molecule, which limits the hydrophilicity of the head-group regions [29].

4.4. Importance of unsaturation of the linoleate chain

Some interesting observations are made: (i) Replacing CER EOS linoleate by CER EOS stearate (saturated chain) prevents the formation of the LPP [54]. Therefore, a high degree of mobility of the C18 chain is a prerequisite for the formation of the LPP. (ii) The (partially) folded linoleate chain in the inner head-group regions can compensate for the long chains of CERs and FFAs from the opposite direction, which extends the central region of the unit cell reaching the opposite head group region approximately at a distance of 10 Å, corresponding to a chain length of ~7–8 C atoms. As the gap between the ester bond of CER EOS and the CH_3 groups of the extended CERs and FFAs is only around 17 Å, while a fully extended linoleate is around 23 Å in length, it is clear that there must be some conformational disordering and/or folding back of the linoleate moiety.

4.5. Further evidence for the proposed location of CER EOS and CHOL in the LPP

Besides CER EOS, CHOL also plays a key role in the formation of the LPP. Previous studies demonstrate that in the absence of CHOL the lipids do not adopt the LPP structure [49,50]. These studies indicate that there is a minimum CHOL content required for the formation of the LPP, corresponding to a CER/CHOL/FFA mole ratio of 1:0.2:1, which gives a CHOL/CER EOS ratio of 1:2. Furthermore, these data also suggest that CHOL not only participates in the formation of the LPP, but also increases the packing density of the lipids in the LPP. Our neutron diffraction studies show that CHOL is located in the outer layer of the LPP with its head-group close to the inner head-group region of the LPP. The positioning of CHOL in this region can fill the gap between the inner head group and the chains of the sphingoid base of CERs and FFAs directing from the unit cell border and may provide increased density in the structure.

Further information obtained from several other studies also supports our proposed model. i) Recently, we observed that the LPP can also be formed using a lipid mixture of less complex composition. Only four lipid (sub)classes are required, that is CER EOS C30, CER NS C24 (0.4:0.6 molar ratio), CHOL and FFA C24 in which the CER/CHOL/FFA are in an equimolar ratio [50]. This indicates that a variation in the head-group architecture of the CER subclasses is not required for the formation of the LPP and therefore a model composed of these four lipid classes as in Fig. 7 is sufficient to show the arrangement. ii) The maximum level of CHOL that can be incorporated in the LPP is 0.5 molar ratio in the CER/CHOL/FFA (1:0.5:1) mixture [50], while a minimum level of 0.2 molar CHOL is required for the formation of the LPP. This reflects certain flexibility in the amount of CHOL that can be incorporated in the crystalline LPP. In addition, in the equimolar CER/CHOL/FFA lipid mixtures, we observed that a gradual increase in CER EOS level results in a gradual increase in the repeat distance of the LPP (unpublished results). This can be explained by the formation of domains of CER EOS surrounded by CHOL interacting with the ester bond of CER EOS (Fig. 7). The partial folding back of the linoleate will fill the gap between the hydroxy group of CHOL and the terminal CH_3 groups of CER NS or FFA present in the central lipid layer. When the level of CER EOS is gradually increased keeping the CHOL level constant, the domains are enlarged and no additional CHOL is required for the formation of the LPP, demonstrating a certain flexibility of the LPP with respect to its CHOL/CER EOS ratio in agreement with the observations. Furthermore, when increasing the level of CER EOS the average additional space for each linoleate moiety provided by the gap between the terminal CH_3 groups of CER NS or FFA and the hydroxy group of CHOL will be reduced. Therefore to create sufficient space for the linoleate an increase in repeat distance is required when increasing the level of CER EOS. iii) As depicted in Fig. 7, when performing studies with only FFA with a chain length of 24 C atoms, CER NS and CER EOS, the CHOL is in an FFA rich (horizontal) layer within the unit cell. In recent studies we observed that the level of FFA is very crucial for the solubility of CHOL (unpublished results). At low FFA levels, the LPP can be formed, but a substantial amount of CHOL phase separates, increasing the FFA level reduced the level of phase separated CHOL drastically, but does not change the formation and repeat distance of the LPP in accordance with our molecular model.

5. Conclusions

In the present study using neutron diffraction, we determined the position of lipids in the unit cell of the LPP. The neutron diffraction reveals the position of CER EOS linoleate and CHOL in the ~130 Å repeating unit: the linoleate moiety is located at the position of the inner head-group regions of the LPP in a highly disorder state while CHOL is located in the outer layer but close to the inner head-group regions of the LPP. The results obtained from our current and previous works provide information on the molecular arrangement of lipids in the unit cell of the LPP and SPP. This information will be beneficial to future studies, allowing detailed studies of the molecular location of other molecules (drug compounds, moisturizers etc.) in the unit cell of these lamellar phases and thereby affording greater insight into the interaction of these agents with the SC lipids.

Transparency document

The Transparency document associated with this article can be found, in online version.

Acknowledgements

We would like to thank the company Evonik (Essen, Germany) for their generous provision of CERs. We also like to thank the personnel at the ILL in Grenoble, France for their assistance and allocation of beam time for neutron diffraction measurements.

Appendix A. Supplementary data

Supplementary data to this article can be found online at http://dx.doi.org/10.1016/j.bbamem.2016.05.006.

References

[1] C. Bonnart, C. Deraison, M. Lacroix, Y. Uchida, C. Besson, A. Robin, A. Briot, M. Gonthier, L. Lamant, P. Dubus, B. Monsarrat, A. Hovnanian, Elastase 2 is expressed in human and mouse epidermis and impairs skin barrier function in Netherton syndrome through filaggrin and lipid misprocessing, J. Clin. Invest. 120 (2010) 871–882 (xE, line, xE, line, xE, lie, xEf).
[2] J.N. Ishikawa, H., N. Kondo, M. Hotta, Y. Takagi, Y. Masukawa, T. Kitahara, Y. Takema, S. Koyano, S. Yamazaki, A. Hatamochi, Changes in the ceramide profile of atopic dermatitis patients, J. Investig. Dermatol. 130 (2010) 2511–2514.
[3] S. Motta, M. Monti, S. Sesana, L. Mellesi, R. Ghidoni, R. Caputo, Abnormality of water barrier function in psoriasis: role of ceramide fractions, Arch. Dermatol. 130 (1994) 452–456.
[4] D.G. Paige, N. Morse-Fisher, J.I. Harper, Quantification of stratum corneum ceramides and lipid envelope ceramides in the hereditary ichthyoses, Br. J. Dermatol. 131 (1994) 23–27.
[5] Y.-H. Park, W.-H. Jang, J.A. Seo, M. Park, T.R. Lee, Y.-H. Park, D.K. Kim, K.-M. Lim, Decrease of ceramides with very long-chain fatty acids and Downregulation of Elongases in a murine atopic dermatitis model, J. Investig. Dermatol. 132 (2012) 476–479.
[6] T.O. Sassa, Y., S. Suzuki, T. Nomura, C. Nishioka, T. Kashiwagi, T. Hirayama, M. Akiyama, R. Taguchi, H. Shimizu, S. Itohara, A. Kihara, Impaired epidermal permeability barrier in mice lacking Elovl1, the Gene responsible for very-long-chain fatty acid production, Mol. Cell. Biol. 33 (2013) 2787–2796.
[7] E. Proksch, J.M. Brandner, J.-M. Jensen, The skin: an indispensable barrier, Exp. Dermatol. 17 (2008) 1063–1072.
[8] P. Talreja, G. Kasting, N. Kleene, W. Pickens, T.-F. Wang, Visualization of the lipid barrier and measurement of lipid pathlength in human stratum corneum, AAPS PharmSci 3 (2001) 48–56.
[9] H.E. Boddé, I. van den Brink, H.K. Koerten, F.H.N. de Haan, Visualization of in vitro percutaneous penetration of mercuric chloride; transport through intercellular space versus cellular uptake through desmosomes, J. Control. Release 15 (1991) 227–236.
[10] H.E. Boddé, M.A.M. Kruithof, J. Brussee, H.K. Koerten, Visualisation of normal and enhanced HgCl2 transport through human skin in vitro, Int. J. Pharm. 53 (1989) 13–24.
[11] P.W. Wertz, M.C. Miethke, S.A. Long, J.S. Strauss, D.T. Downing, The composition of the ceramides from human stratum corneum and from Comedones, J. Investig. Dermatol. 84 (1985) 410–412.
[12] K.J. Robson, M.E. Stewart, S. Michelsen, N.D. Lazo, D.T. Downing, 6-hydroxy-4-sphingenine in human epidermal ceramides, J. Lipid Res. 35 (1994) 2060–2068.
[13] M.E. Stewart, D.T. Downing, A new 6-hydroxy-4-sphingenine-containing ceramide in human skin, J. Lipid Res. 40 (1999) 1434–1439.
[14] Y. Masukawa, H. Narita, E. Shimizu, N. Kondo, Y. Sugai, T. Oba, R. Homma, J. Ishikawa, Y. Takagi, T. Kitahara, Y. Takema, K. Kita, Characterization of overall ceramide species in human stratum corneum, J. Lipid Res. 49 (2008) 1466–1476.
[15] A. Weerheim, M. Ponec, Determination of stratum corneum lipid profile by tape stripping in combination with high-performance thin-layer chromatography, Arch. Dermatol. Res. 293 (2001) 191–199.
[16] M. Rabionet, K. Gorgas, R. Sandhoff, Ceramide synthesis in the epidermis, Biochim. Biophys. Acta, Mol. Cell. Biol. Lipids 1841 (2014) 422–434.
[17] J. van Smeden, L. Hoppel, R. van der Heijden, T. Hankemeier, R.J. Vreeken, J.A. Bouwstra, LC/MS analysis of stratum corneum lipids: ceramide profiling and discovery, J. Lipid Res. 52 (2011) 1211–1221.
[18] M. Ponec, A. Weerheim, P. Lankhorst, P. Wertz, New Acylceramide in native and reconstructed epidermis, J. Investig. Dermatol. 120 (2003) 581–588.
[19] J.A. Bouwstra, G.S. Gooris, J.A. van der Spek, W. Bras, Structural investigations of human stratum corneum by small-angle X-ray scattering, J. Investig. Dermatol. 97 (1991) 1005–1012.
[20] K.C. Madison, D.C. Swartzendruber, P.W. Wertz, D.T. Downing, Presence of intact intercellular lipid lamellae in the upper layers of the stratum corneum, J. Investig. Dermatol. 88 (1987) 714–718.
[21] S.H. White, D. Mirejovsky, G.I. King, Structure of lamellar lipid domains and corneocyte envelopes of murine stratum corneum. An x-ray diffraction study, Biochemistry 27 (1988) 3725–3732.
[22] I. Hatta, N. Ohta, K. Inoue, N. Yagi, Coexistence of two domains in intercellular lipid matrix of stratum corneum, Biochim. Biophys. Acta Biomembr. 1758 (2006) 1830–1836.
[23] M.W. de Jager, G.S. Gooris, I.P. Dolbnya, W. Bras, M. Ponec, J.A. Bouwstra, Novel lipid mixtures based on synthetic ceramides reproduce the unique stratum corneum lipid organization, J. Lipid Res. 45 (2004) 923–932.
[24] M. Janssens, J. van Smeden, G.S. Gooris, W. Bras, G. Portale, P.J. Caspers, R.J. Vreeken, T. Hankemeier, S. Kezic, R. Wolterbeek, A.P. Lavrijsen, J.A. Bouwstra, Increase in short-chain ceramides correlates with an altered lipid organization and decreased barrier function in atopic eczema patients, J. Lipid Res. 53 (2012) 2755–2766.
[25] E.H. Mojumdar, D. Groen, G.S. Gooris, D.J. Barlow, M.J. Lawrence, B. Deme, J.A. Bouwstra, Localization of cholesterol and fatty acid in a model lipid membrane: a neutron diffraction approach, Biophys. J. 105 (2013) 911–918.
[26] A. Schröter, D. Kessner, M.A. Kiselev, T. Hauß, S. Dante, R.H.H. Neubert, Basic nanostructure of stratum corneum lipid matrices based on ceramides [EOS] and [AP]: a neutron diffraction study, Biophys. J. 97 (2009) 1104–1114.
[27] D. Kessner, M. Kiselev, S. Dante, T. Hauß, P. Lersch, S. Wartewig, R.H. Neubert, Arrangement of ceramide [EOS] in a stratum corneum lipid model matrix: new aspects revealed by neutron diffraction studies, Eur. Biophys. J. 37 (2008) 989–999.
[28] A. Ruettinger, M. Kiselev, T. Hauss, S. Dante, A. Balagurov, R. Neubert, Fatty acid interdigitation in stratum corneum model membranes: a neutron diffraction study, Eur. Biophys. J. 37 (2008) 759–771.
[29] D. Groen, G.S. Gooris, D.J. Barlow, M.J. Lawrence, J.B. van Mechelen, B. Demé, J.A. Bouwstra, Disposition of ceramide in model lipid membranes determined by neutron diffraction, Biophys. J. 100 (2011) 1481–1489.
[30] I. Iwai, H. Han, L.d. Hollander, S. Svensson, L.-G. Ofverstedt, J. Anwar, J. Brewer, M. Bloksgaard, A. Laloeuf, D. Nosek, S. Masich, L.A. Bagatolli, U. Skoglund, L. Norlen, The human skin barrier is organized as stacked bilayers of fully extended ceramides with cholesterol molecules associated with the ceramide sphingoid moiety, J. Investig. Dermatol. 132 (2012) 2215–2225.
[31] T.J. McIntosh, Organization of Skin Stratum Corneum Extracellular Lamellae: diffraction evidence for asymmetric distribution of cholesterol, Biophys. J. 85 (2003) 1675–1681.
[32] D. Groen, G.S. Gooris, J.A. Bouwstra, New insights into the stratum corneum lipid organization by X-ray diffraction analysis, Biophys. J. 97 (2009) 2242–2249.
[33] E.H. Mojumdar, G.S. Gooris, D.J. Barlow, M.J. Lawrence, B. Deme, J.A. Bouwstra, Skin lipids: localization of ceramide and fatty acid in the unit cell of the long periodicity phase, Biophys. J. 108 (2015) 2670–2679.
[34] J.A. Bouwstra, G.S. Gooris, K. Cheng, A. Weerheim, W. Bras, M. Ponec, Phase behavior of isolated skin lipids, J. Lipid Res. 37 (1996) 999–1011.
[35] P.W. Wertz, D.T. Downing, Epidermal lipids, in: L.A. Goldsmith (Ed.), Physiology, Biochemistry, and Molecular Biology of the Skin, Oxford University Press, New York 1991, pp. 205–236.
[36] D. Richard, http://www.ill.eu/instruments-support/computing-for-science/data-analysis/ (Accessed May 2010) 2008.
[37] N.P. Franks, W.R. Lieb, The structure of lipid bilayers and the effects of general anaesthetics: an X-ray and neutron diffraction study, J. Mol. Biol. 133 (1979) 469–500.
[38] NCNR, http://www.ncnr.nist.gov/instruments/bt1/neutron.html (Accessed:May 2010) 2005.
[39] D.L. Worcester, N.P. Franks, Structural analysis of hydrated egg lecithin and cholesterol bilayers II. Neutron diffraction, J. Mol. Biol. 100 (1976) 359–378.
[40] J.F. Nagle, S. Tristram-Nagle, Structure of lipid bilayers, Biochim. Biophys. Acta Rev. Biomembr. 1469 (2000) 159–195.
[41] T.A. Harroun, J. Katsaras, S.R. Wassall, Cholesterol hydroxyl group is found to reside in the Center of a Polyunsaturated Lipid Membrane, Biochemistry 45 (2006) 1227–1233.
[42] NCNR, http://www.ncnr.nist.gov/resources/activation/2014.
[43] M.C. Wiener, S.H. White, Fluid bilayer structure determination by the combined use of x-ray and neutron diffraction. II. "composition-space" refinement method, Biophys. J. 59 (1991) 174–185.
[44] M.C. Wiener, G.I. King, S.H. White, Structure of a fluid dioleoylphosphatidylcholine bilayer determined by joint refinement of x-ray and neutron diffraction data. I. Scaling of neutron data and the distributions of double bonds and water, Biophys. J. 60 (1991) 568–576.
[45] R.E. Jacobs, S.H. White, The nature of the hydrophobic binding of small peptides at the bilayer interface: implications for the insertion of transbilayer helices, Biochemistry 28 (1989) 3421–3437.
[46] G. Zaccai, J.K. Blasie, B.P. Schoenborn, Neutron diffraction studies on the location of water in lecithin bilayer model membranes, Proc. Natl. Acad. Sci. 72 (1975) 376–380.
[47] J.A. Bouwstra, K. Cheng, G.S. Gooris, A. Weerheim, M. Ponec, The role of ceramides 1 and 2 in the stratum corneum lipid organisation, Biochim. Biophys. Acta, Lipids Lipid Metab. 1300 (1996) 177–186.
[48] J.A. Bouwstra, G.S. Gooris, F.E.R. Dubbelaar, A.M. Weerheim, A.P. IJzerman, M. Ponec, Role of ceramide 1 in the molecular organization of the stratum corneum lipids, J. Lipid Res. 39 (1998) 186–196.
[49] T.J. McIntosh, M.E. Stewart, D.T. Downing, X-ray diffraction analysis of isolated skin lipids: reconstitution of intercellular lipid domains, Biochemistry 35 (1996) 3649–3653.
[50] E.H. Mojumdar, G.S. Gooris, J. Bouwstra, Phase behavior of skin lipid mixtures: effect of cholesterol on the lipid organization, Soft Matter 11 (2015) 4326–4336.
[51] M. de Jager, G. Gooris, M. Ponec, J. Bouwstra, Acylceramide head group architecture affects lipid organization in synthetic ceramide mixtures, J. Investig. Dermatol. 123 (2004) 911–916.
[52] M.A. Kiselev, N.Y. Ryabova, A.M. Balagurov, S. Dante, T. Hauss, J. Zbytovska, S. Wartewig, R.H.H. Neubert, New insights into the structure and hydration of a stratum corneum lipid model membrane by neutron diffraction, Eur. Biophys. J. 34 (2005) 1030–1040.
[53] M. Janssens, G.S. Gooris, J.A. Bouwstra, Infrared spectroscopy studies of mixtures prepared with synthetic ceramides varying in head group architecture: coexistence of liquid and crystalline phases, Biochim. Biophys. Acta Biomembr. 1788 (2009) 732–742.
[54] D. de Sousa Neto, G. Gooris, J. Bouwstra, Effect of the ω-acylceramides on the lipid organization of stratum corneum model membranes evaluated by X-ray diffraction and FTIR studies (part I), Chem. Phys. Lipids 164 (2011) 184–195.